ACS APPLIED MATERIALS & INTERFACES

Research Article

www.acsami.org

# Casein-Coated Iron Oxide Nanoparticles for High MRI Contrast Enhancement and Efficient Cell Targeting

Jing Huang,[†] Liya Wang,[†] Run Lin,[†,‡] Andrew Y. Wang,[§] Lily Yang,[⊥,∥] Min Kuang,[§] Weiping Qian,[⊥] and Hui Mao*,[†,∥]

[†]Department of Radiology and Imaging Sciences and [⊥]Department of Surgery, Emory University School of Medicine, Atlanta, Georgia 30322, United States

[‡]Department of Interventional Radiology, Sun Ye-Tzen University School of Medicine, Guangzhou, Guangdong 510080, China

[§]Ocean NanoTech, LLC, Springdale, Arkansas 72764, United States

[∥]Winship Cancer Institute, Emory University, Atlanta, Georgia 30322, United States

Supporting Information

**ABSTRACT:** Surface properties, as well as inherent physicochemical properties, of the engineered nanomaterials play important roles in their interactions with the biological systems, which eventually affect their efficiency in diagnostic and therapeutic applications. Here we report a new class of MRI contrast agent based on milk casein protein-coated iron oxide nanoparticles (CNIOs) with a core size of 15 nm and hydrodynamic diameter ~30 nm. These CNIOs exhibited excellent water-solubility, colloidal stability, and biocompatibility. Importantly, CNIOs exhibited prominent $T_2$ enhancing capability with a transverse relaxivity $r_2$ of 273 $mM^{-1}$ $s^{-1}$ at 3 tesla. The transverse relaxivity is ~2.5-fold higher than that of iron oxide nanoparticles with the same core but an amphiphilic polymer coating. CNIOs showed pH-responsive properties, formed loose and soluble aggregates near the pI (pH ~4.0). The aggregates could be dissociated reversibly when the solution pH was adjusted away from the pI. The transverse relaxation property and MRI contrast enhancing effect of CNIOs remained unchanged in the pH range of 2.0−8.0. Further functionalization of CNIOs can be achieved via surface modification of the protein coating. Bioaffinitive ligands, such as a single chain fragment from the antibody of epidermal growth factor receptor (ScFvEGFR), could be readily conjugated onto the protein coating, enabling specific targeting to MDA-MB-231 breast cancer cells overexpressing EGFR. $T_2$-weighted MRI of mice intravenously administered with CNIOs demonstrated strong contrast enhancement in the liver and spleen. These favorable properties suggest CNIOs as a class of biomarker targeted magnetic nanoparticles for MRI contrast enhancement and related biomedical applications.

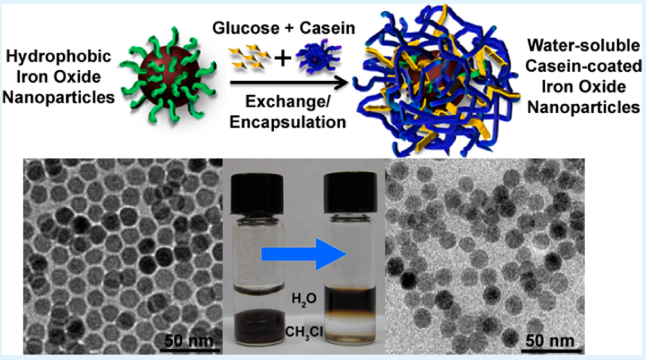


**KEYWORDS:** *iron oxide nanoparticles, magnetic resonance imaging, casein, contrast agent, targeting*

## INTRODUCTION

Magnetic iron oxide (IO, i.e., $Fe_3O_4$, $\gamma$-$Fe_2O_3$) nanoparticles have attracted extensive attention because of their biomedical applications in cell labeling, magnetic resonance imaging (MRI), and imaging-guided drug delivery.[1−5] IO nanoparticles synthesized via pyrolysis of organometallic iron precursors possess high uniformity and excellent magnetic properties. However, because of the inevitable hydrophobic residues (i.e., oleic acid) on the surface, they have poor water solubility for biomedical applications. Increasing efforts are devoted to fabricate biocompatible IO nanoparticles with functional coatings, including synthetic polymers and natural products (e.g., proteins). Conventionally, the phase transfer process of high-quality hydrophobic IO nanoparticles to aqueous phase is based on exchanging surface surfactants with amphiphilic molecules, such as polyethylene glycol (PEG), PEG phospholipid, dextran, poly(acrylic acid) (PAA), polyethylenimine (PEI), or glutathione (GSH), etc.[6−11] However, this exchange method usually requires reactions (heating or sonicating) between IO nanoparticles and coating materials in a dipolar solvent (e.g., dimethyl sulfoxide, DMSO), and is not applicable for protein coating. Although IO-protein complex could be fabricated through directly mixing the aqueous protein solution and hydrophobic IO nanoparticles, large clusters may form because of the incompatibility of those two components.[12] In addition, biomimetic magnetic nanoparticles can be formed by coprecipitating ferric and ferrous salt inside protein cages, or postsynthesis encapsulating.[13−18] However, the biomineraliza-

Received: August 18, 2012
Accepted: April 30, 2013
Published: April 30, 2013

  

tion or coprecipitation under mild conditions typically yields magnetic nanoparticles with limited magnetic properties. Therefore, a simple and reliable strategy for fabricating protein-coated IO nanoparticles needs to be developed.

Casein (CN) is a main ingredient (~80%) of bovine milk that contains several related phosphoproteins. Specifically, bovine casein is consisted of four types of phosphoproteins (i.e., $\alpha S_1$-, $\alpha S_2$-, $\beta$-, and $\kappa$-CN) with molecular weight of 19−25 kDa, and an isoelectric point (pI) of 4.2−5.8.[19,20] Casein has a high affinity for binding ions or small molecules. Naturally, casein self-assembles into micelles with diameters ranging from 50 to 500 nm, acting as natural nanovehicles for delivery of calcium, phosphate and other biomolecules.[21−26] Generally, the casein micelle is believed to be formed based on the open structure and distinct hydrophobic/hydrophilic domains of these proline-rich phosphoproteins, which allow casein to change its conformation easily in solution. Casein micelle is stabilized by an out layer of hair-like $\kappa$-casein molecules, which protrude their hydrophilic C-terminal domains into the aqueous environment. In addition to its excellent biocompatibility and biodegradability, casein has pH-responsive structural, conformational, and functional changes, and is heat-stable up to 60−70 °C.[27−29] These unique structural and physicochemical properties have led to the earlier studies of casein-based drug delivery systems.[30−36]

In this work, we report the development of casein-coated iron oxide nanoparticles (CNIOs) for biomarker targeted MRI. Because conventional exchange methods require harsh reaction conditions which can easily denature proteins and deform the nanoparticle surface structure, we use a recently developed exchange-encapsulation method to transfer high quality hydrophobic IO nanoparticles to the aqueous phase.[37] This process, as illustrated in Scheme 1, is mediated by a widely available

**Scheme 1. Illustration of the Exchange-Encapsulation Process for Coating Iron Oxide (IO) Nanoparticles with Casein to Obtain Casein Coated Iron Oxide Nanoparticles (CNIO)**

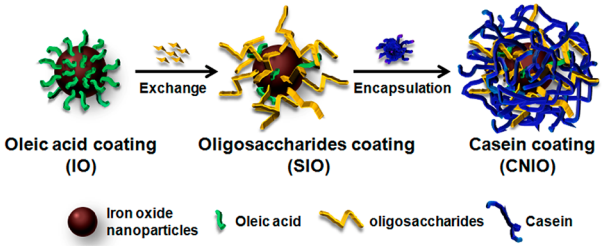


natural nutrient molecule, glucose, which can be oxidized and polymerized into oligosaccharides under high temperature conditions.[38,39] For the current study these oligosaccharide molecules partially replace oleic acid and protect hydrophobic IO nanoparticles from oxidation during the exchange procedure. The ionic oligosaccharide renders hydrophilic moieties of protein molecules onto the surface of IO nanoparticle cores. This new approach allows the robust preparation of nanomaterials with a desired protein coating, resulted in water-soluble and stable nanocolloids for biomedical applications. Such milk protein-coated iron oxide nanoparticles exhibit a significantly higher transverse relaxivity than that of the same nanoparticulate core coated with synthetic polymer, providing a highly efficient MRI contrast agent. More importantly, bioaffinitive ligands, such as single chain fragment from the antibody of epidermal growth factor receptor (ScFvEGFR), can be readily conjugated onto the protein coating, enabling specific targeting to tumor cells for targeted molecular imaging and drug delivery applications.

## MATERIALS AND METHODS

**Materials.** All materials were used as received. Bovine casein, glucose, glutaradehyde, *N*,*N*-dimethylformamide (DMF), dimethyl sulfoxide (DMSO), 3-[4,5-dimethylthiazol-2-yl]-2,5-diphenyltetrazolium bromide (MTT) were purchased from Sigma-Aldrich (St. Louis, MO). 1-Ethyl-3-[3-dimethylaminopropyl]carbodiimide hydrochloride (EDC), *N*-hydroxysulfosuccinimide (Sulfo-NHS) were obtained from Thermo Scientific (Rockford, IL). All cell culture materials (media and supplements) were purchased from Invitrogen (Burlington, ON). 100 kDa MWCO Ultra-4 centrifuge tubes were purchased from Millipore (Billerica, MA).

**Synthesis of Casein-Coated Iron Oxide Nanoparticles (CNIOs).** Hydrophobic IO nanoparticles were prepared by heating iron oxide powder and oleic acid in octadecene at 315 °C.[40] To transfer IO nanoparticles into aqueous phase, a chloroform solution of IO nanoparticles was added to a preheated glucose/DMF solution with a molar ratio of IO nanoparticle:glucose at $1:1 \times 10^5$. The mixture was refluxed for 1 h, and then cooled to room temperature. IO nanoparticles were precipitated with ethanol and then separated by SuperMag Separator (Ocean Nanotech, Springdale, AR), washed three times with ethanol. The resulted IO nanoparticles were redispersed in water, which turned into a brownish solution. Casein was pretreated with 0.01 M NaOH solution to form soluble base. The treated casein powder was added into the IO nanoparticle solution with a molar ratio of IO nanoparticle: casein at 1:200. The mixture was shaken gently at room temperature for about 4 h. Freshly prepared glutaradehyde solution (0.4%, with the molar ratio of glutaradehyde:casein at 1:2) was then added dropwise into the above mixture solution under magnetic stirring. This cross-link reaction was allowed to proceed for 1 h. The resulting CNIO product was washed with water several times through Ultra-4 centrifuge tubes with a cut off size of 100 kDa, then collected by magnetic separation and redispersed in water. The stock solution of CNIOs was stored at 4 °C for further use. The pH-dependent tests were conducted by adjusting the CNIO dispersion with diluted HCl or NaOH. The pH adjusted CNIO dispersions were then gently shaken at room temperature for 1 h to allow the sufficient reformation. The hydrodynamic size, surface charge, and MRI relaxation properties of the particles were studied to investigate the pH dependent stability of CNIOs.

**Characterization of CNIOs.** The morphology and size of CNIOs were studied using transmission electron microscope (TEM, Hitachi H-7500 accelerating voltage 75 kV). Typically, TEM samples were prepared by dropping diluted nanoparticle solutions on a carbon coated copper grid and air-dried. For the negative staining, 1% phosphotungstic acid (PTA) aqueous solution was used to stain the background to visualize the protein coating, after a drop of CNIO solution was deposited on the copper grid and the solvent was wicked away. The hydrodynamic size (in diameter) and surface charge of nanoparticles in the aqueous solution were evaluated using a dynamic light scattering (DLS) instrument (Malvern Zeta Sizer Nano S-90) equipped with a 22 mW He−Ne laser operating at 632.8 nm. The averaged sizes were obtained from three measurements (10 runs per measurement) for each sample using number-weighted statistics. The Fourier transform infrared spectroscopy (FTIR) spectra were collected on a PerkinElmer Spectrum 100 FT-IR spectrometer (Bucks, UK). UV−vis absorption spectra were obtained with a scanning spectrophotometer (Shimadzu UV-2401PC) with a slit width of 1.0 nm.

**Measurements of Transverse Relaxation Time and Relaxivity.** The transverse relaxation, or $T_2$, properties of CNIOs at different pH conditions were determined using a 3T MRI scanner (Magnetom Tim Trio, Siemens Medical Solutions, Erlangen, Germany). Solutions of CNIOs and amphiphlic polymer-coated iron oxide nanoparticles (SHP15),[6] which have the same iron oxide core as


dx.doi.org/10.1021/am400713j | ACS Appl. Mater. Interfaces 2013, 5, 4632−4639

CNIO, were prepared with Fe concentrations varying from 0.006 to 0.089 mM. The phantom tubes containing those solution samples were placed in the MRI scanner. A $T_2$-weighted fast spin echo imaging sequence with a repetition time (TR) of 3200 ms and echo time (TE) of 60 ms was used to evaluate the contrast effect of different nanoparticle solutions. To measure the transverse relaxation time $T_2$, a multiecho spin echo sequence was used with a TR of 2000 ms and 20 different TEs, starting at 10 ms with increments of 10 ms. Signal intensity (SI) of each region of interest (ROI) was measured for each concentration at different TEs. The values of $T_2$ relaxation times at different concentrations were derived from the fitting of the average SI data using a nonlinear exponential equation.[11]

**Cytotoxicity Evaluation.** Cytotoxicity of CNIOs was assessed in vitro by the 3-(4,5-dimethylthiazol-2-yl)-2,5-iphenyltetrazolium bromide (MTT) assay. Mouse macrophage RAW264.7 cells were detached and seeded in 96-well flat-bottom microplates at 5,000 cells per well. After 24 h recovery at 37 °C, the medium was replaced with 200 $\mu$L medium containing CNIOs at various concentrations (5, 10, 20, 50, 100, and 200 $\mu$g Fe/mL). For the control sample, fresh medium without CNIOs was added. After 24 h of incubation at 37 °C, 20 $\mu$L of MTT solution (5 mg/mL) was added into each well following a 3 h of incubation. After removing the culture media, the precipitated formazan was then dissolved in DMSO. Finally, a microplate reader (Biotech Synergy2) was used to measure the absorbance of all samples ($n$ = 5 per group) at 540 nm. Cell viability was determined by comparing the absorbance of cells incubated with CNIOs to that of the control cells incubated without CNIOs.

**MRI of CNIOs in Mice.** All animal experiments were conducted following a protocol approved by Institutional Animal Care and Use Committee (IACUC). CNIOs were injected into Balb/c mice ($n$ = 3) through the tail vein at a dosage of 2.5 mg Fe/kg of mouse body weight. Animals were anesthetized by i.p. injection of a ketamine-xylazine mixture (95:5 mg/kg) before being placed in a 3T MRI scanner. $T_2$-weighted fast spin echo images were acquired using a volumetric wrist coil in the coronal sections covering the whole mouse body before and 20, 40, 60, and 150 min and 24 and 48 h after injection of nanoparticle contrast agents. The imaging parameters included: TR of 3600 ms, TE of 32 ms, matrix of 320 × 128, field of view (FOV) of 120 × 60 mm$^2$, flip angle of 150°, and slice thickness of 1.00 mm. The signal-to-noise ratio (SNR) was calculated according to the equation: $SNR = SI_{mean}/SD_{noise}$. The relative contrast enhancement at each time point was defined as signal decrease $\Delta SNR = (SNR_{pre} - SNR_{post})/SNR_{pre}$.

**Conjugation of CNIOs with an EGFR Targeting Ligand.** The human EGFR specific single chain fragment of anti-EGFR antibody (ScFvEGFR) expressing plasmid (ScFv B10) was kindly provided by Dr. Gregory Adams at Fox Chase Cancer Center, Philadelphia, PA. The ScFvEGFR of anti-EGFR antibody was produced using an established procedure published previously[41] and then conjugated to CNIOs via a covalent link of the carboxyl group of ScFvEGFR and the amine group of casein coating.[42,43] Briefly, ScFvEGFR (1 mg) was reacted with NHS (0.25 mg) and EDAC (0.5 mg) in MES buffer solution (1 M, pH 5.5) for 15 min. Then CNIOs dispersed in borate buffer solution (0.5 M, pH 8.5) was added. The mixture was allowed to react for 2 h. The product was collected by SuperMag Separator and washed with deionized water.

**Specific Cell Binding of ScFvEGFR-CNIOs.** Breast cancer MDA-MB-231 (overexpressing EGFR) and MCF7 (expressing EGFR at a very low level) cells were seeded in 8-well chamber slides at the concentration of 50,000 cells per well. After recovering for 24 h, the media was replaced with that contained ScFvEGFR-CNIOs at the concentrations of 0, 0.10, and 0.25 mg Fe/mL. Cells were incubated at 37 °C for 4 h. The cell monolayer was then rinsed with PBS, and fixed with 4% paraformaldehyde in PBS solution. Prussian blue staining for iron was performed to investigate the specific binding of ScFvEGFR-CNIOs to cells with EGFR expression. Briefly, freshly prepared 10% potassium ferrocyanide (II) trihydrate and 20% HCl solution were mixed together and added to wells containing fixed cells. After incubating for 1 h, the working solution was removed, and the cells were washed with PBS. Counterstaining was performed by adding the nuclear fast red solution and incubating for 5 min. The cells were then dehydrated with 70% and 100% ethanol and rinsed in xylene. The slides were mounted and examined by a light microscope.

## RESULTS AND DISCUSSION

**Synthesis and Characterization of CNIOs.** The hydrophobic IOs with a core size of 15.1 ± 0.6 nm (diameter), as shown in the TEM image in Figure 1a, were coated with oleic

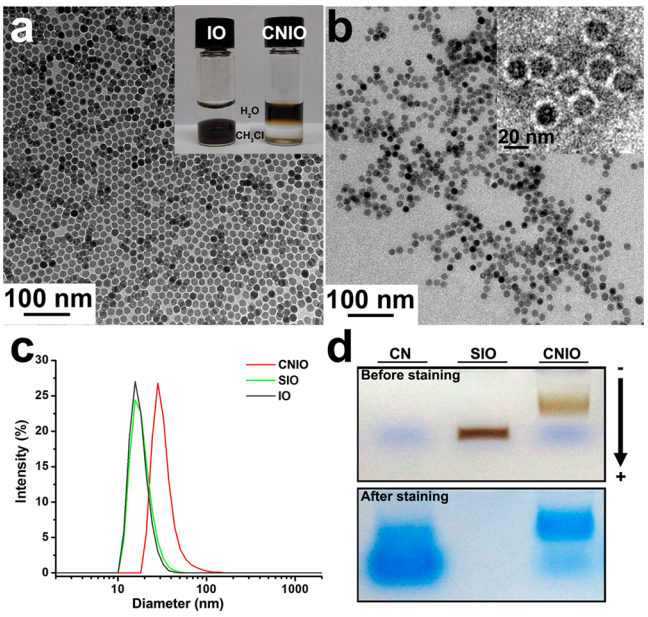


**Figure 1.** TEM images of (a) hydrophobic IO nanoparticles before modification and (b) after being coated with casein (CNIOs). Inset of a is a photograph of hydrophobic IO nanoparticles dispersed in chloroform (left) and water-soluble CNIOs (right); inset of b is a negative stained TEM image that shows a protein coating (bright layer surrounding the particles); (c) dynamic light scattering (DLS) data showing the changes of hydrodynamic size (in diameter) of IO nanoparticles before modification, after ligand exchange, and after being coated with casein; (d) pictures of gel electrophoresis analysis of casein (CN), oligosaccharide coated iron oxide nanoparticles (SIO), casein-coated iron oxide nanoparticles (CNIO) with a gel running marker (frontier, DNA loading dye) (top panel), and corresponding gel code blue staining (bottom panel).

acid and only soluble in nonpolar solvent (e.g., chloroform, hexane). After oleic acid was exchanged with oligosaccharides, IO nanoparticles were subsequently coated with casein to obtain water-soluble CNIOs (inset in Figure 1a). TEM measurement showed that the core size of CNIOs remained unchanged (~15 nm) after the ligand exchange process (Figure 1b). However, the number-weighted hydrodynamic diameter of nanoparticles changed from 17.6 to 18.5 nm after exchanging with oligosaccharides, and further increased to 30.5 nm after the formation of casein coating (Figure 1c). The changes in hydrodynamic size suggested the expected transition of different types of surface coating at different stages in the preparation. Negative staining allowed for visualizing a layer of 4-nm thick protein coating around the IO nanoparticles (inset in Figure 1b). Successful coating of casein molecules onto the nanoparticle surface was further confirmed by the surface charge changes. The surface zeta potential changed from −18.8 ± 4.9 mV to −38.0 ± 3.9 mV after attachment of casein proteins. The substantial increase in negative surface charge is likely attributed to the presence of a large number of carboxyl


dx.doi.org/10.1021/am400713j | ACS Appl. Mater. Interfaces 2013, 5, 4632−4639

groups in casein. Size exclusion gel electrophoresis was used to determine the amount and purity of the obtained CNIOs. CNIOs exhibited a slower moving band (Figure 1d), compared to that of the IO nanoparticles without casein coating, indicating the increased size of CNIOs after the protein encapsulation. Gel code blue staining, which stains for the presence of casein, further confirmed the casein coating on the CNIO sample with a strong blue band in the location corresponding to CNIOs. No such blue band was observed for the IO nanoparticles without casein coating because of the absence of protein.

Fourier transform infrared (FTIR) spectra were acquired for further demonstration of the presence of casein coating on CNIOs (Figure 2). A characteristic peak from the Fe−O

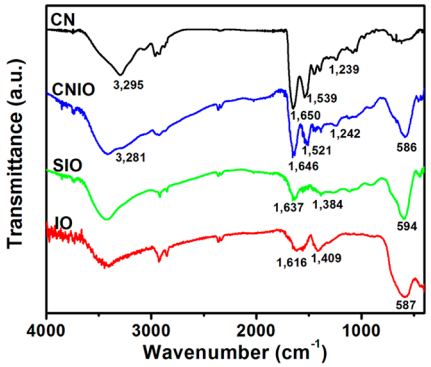


**Figure 2.** FT-IR spectra of hydrophobic iron oxide (IO) nanoparticles, oligosaccharide-coated iron oxide (SIO) nanoparticles, casein-coated iron oxide (CNIO) nanoparticles and casein (CN).

stretching band of iron oxide was observed at 586 $cm^{-1}$. The formation of casein coating on the nanoparticles was confirmed by the characteristic peaks from amide bands of protein in the IR spectra of CNIOs, compared with pure casein. Peaks at 1646 and 1521 $cm^{-1}$ referred to C═O and C−N stretching from amide I and II, and the band at 1300−1200 $cm^{-1}$ referred to C−N stretching and N−H deformation. In comparison with CNIOs, the IR spectra of oleic acid and oligosaccharides coated IO nanoparticles only displayed peaks from C═C stretching (1616 $cm^{-1}$ for IO, 1637 $cm^{-1}$ for SIO) and C−H bending (1409 $cm^{-1}$ for IO, 1384 $cm^{-1}$ for SIO). Using the Bradford assay which measures the protein content, we estimated that approximately 50 casein molecules were assembled on each IO nanoparticle.

Prepared CNIOs were easily dispersed in the aqueous solution. Aqueous CNIOs suspension was stable for months in storage at 4 °C without noticeable precipitation. Furthermore, the hydrodynamic size of CNIOs remained unchanged after 48 h incubation in the physiological condition of either phosphate buffer (PBS, pH 7.4) or serum-contained cell culture medium at room temperature (Figure 3).

**MRI Relaxation Properties of CNIOs.** To evaluate the MRI contrast enhancing capability of CNIOs, the transverse relaxivity and MRI signal changes of aqueous CNIO solutions with different Fe concentrations were investigated on a 3T MRI scanner. For comparison, amphiphilic polymer coated iron oxide nanoparticles (SHP15, with carboxyl groups on the surface, −30 to −50 mV) with the same core size (15 nm) were selected.[6] As shown in Figure 4a, substantially stronger hypointense contrast in $T_2$-weighted spin echo images were observed in CNIO samples compared to those of SHP15 at the

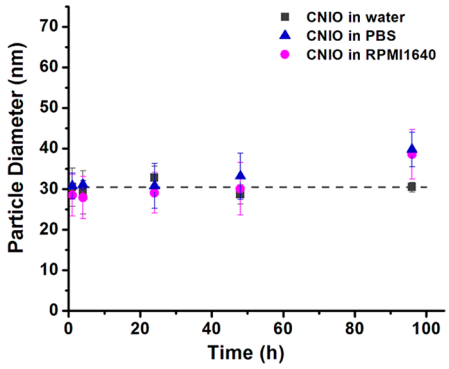


**Figure 3.** Stability of CNIOs in water, PBS, and RPMI1640 culture medium as assessed by DLS. The particle size did not show significant change after 48 h incubation in those mediums at room temperature.

same iron concentrations. The decrease of MRI signal in $T_2$-weighted images was iron concentration dependent. Transverse relaxation time $T_2$ at each iron concentration were determined by fitting the MRI signal intensities at different echo times ($n$ = 20) with an exponential function. Transverse relaxivity $r_2$ was calculated from slopes of the linear correlation between the relaxation rates (i.e., $1/T_2$) and iron concentrations (Figure 4b). The calculated $r_2$ was 273 $mM^{-1}$ $s^{-1}$ for CNIOs, compared to 109 $mM^{-1}$ $s^{-1}$ for SHP15. Thus, with casein coating, CNIOs exhibited an $r_2$ almost 2.5-fold higher than that of SHP15 coated with amphiphilic polymer. The increase in $r_2$ for CNIOs was further confirmed by the magnetic susceptibility measurement (see Figure S4 in the Supporting Information). The complex susceptibility for CNIOs is 0.043 at the frequency 1000 Hz, which is 1.4 times higher than that of SHP15 (~0.030). The increased relaxivity may lead to higher sensitivity for detecting abnormalities, allowing for the same imaging quality at a reduced dosage with less toxicity concern.

Importantly, the increase in $r_2$ of CNIOs suggests that the coating material and surface properties play important roles in modulating MRI contrast enhancing effect. The unique structure and properties of casein changed the interface between the nanoparticle and bulk water medium. As it is known, the dipolar interactions between the particle magnetic moments and the surrounding water protons contribute to the shortening of the $T_2$ relaxation time and proton dephasing. The higher and more efficient MRI contrast from CNIOs is possibly caused by the high water permeability of the coating, allowing water molecules to access and diffuse in and out of the inner/outer layers. Meanwhile, the high affinity of casein coating to water molecules may promote the interactions and diffusion of surrounding water molecules around the particles.[44,45] Moreover, casein molecules have abundant hydrate function groups that can increase the exchange between the hydrated water molecules and ones in bulky surrounding. Another possible interpretation for the substantially increased $r_2$ is that some casein molecules may be covalently conjugated to the particle surface through the phosphate groups,[46] reducing the exclusion of water molecules from the particle surface and facilitating the exchange between bulk water and those residing on the casein surface. Similar phenomena were observed from human serum albumin and other protein coated IO nanoparticles.[47,48] In addition to the hydrophilicity and water diffusion effect of the coating materials, less surface defects or deformation in the reductive environment during the modification may also contribute to the higher MRI contrast enhancement.


dx.doi.org/10.1021/am400713j | ACS Appl. Mater. Interfaces 2013, 5, 4632−4639

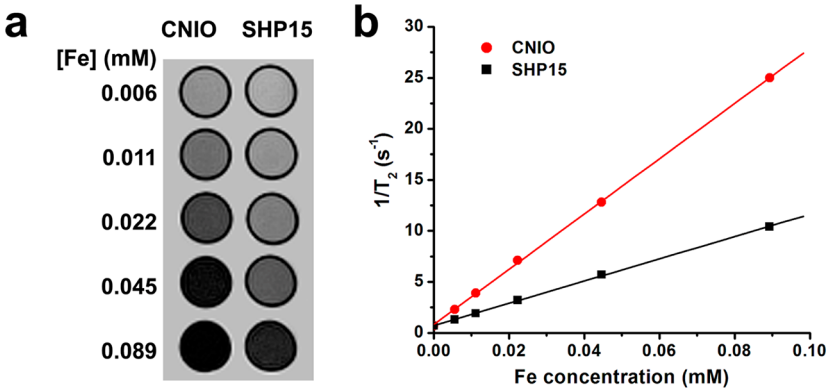


**Figure 4.** (a) $T_2$-weighted spin echo MR images of CNIOs and SHP15 at different concentrations; (b) transverse relaxation rates ($1/T_2$, $s^{-1}$) of CNIOs and SHP15 as a function of the iron concentration (mM).

**pH-Responsive Properties of CNIOs.** Similar to pure CN (pI ~4.2−5.8),[20] CNIOs were found to be highly pH-responsive and exhibit U-shaped dispersibility as a function of pH. Zeta potential measurements showed that the surface charge of CNIOs shifted from negative to positive as the pH value decreased from 8.0 to 2.0 (Figure 5a). This shift was

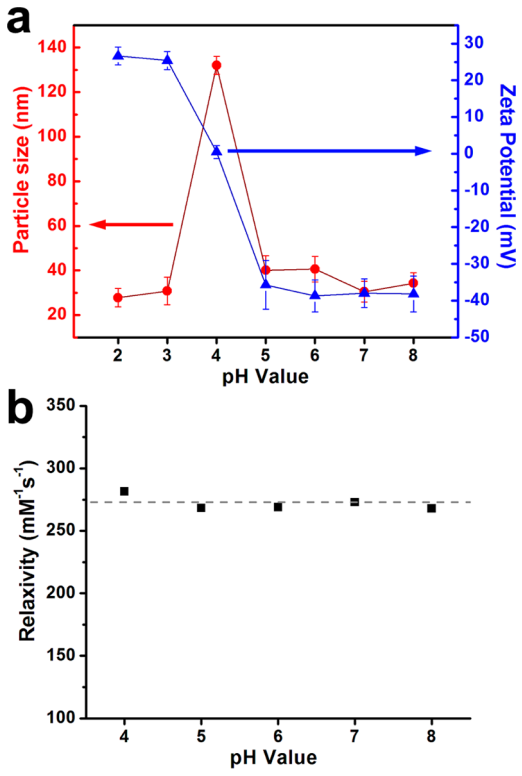


**Figure 5.** (a) Plots of changes in hydrodynamic size (red solid cycle) and surface charge (blue triangle) of CNIOs as a function of pH; (b) transverse relaxivity $r_2$ of CNIOs as a function of pH.

caused by the neutralization of negative surface charge due to the pH decrease. The isoelectric point (pI) for CNIOs was determined to be ~pH 4.0, when the surface charge was neutralized to zero. The electrostatic repulsion between the particles decreased, thus leading to the aggregation of CNIOs. As shown in DLS data, particle sizes increased from 30.5 nm (pH 7.0) to 132 nm (pH 4.0) by forming loose aggregates. When the pH was decreased further, from 4.0 to 2.0, the surface charge became positive (~25.4 mV), providing sufficient electrostatic repulsion between particles, and thus promoted the dissociation of aggregates and the recovery of single dispersion with a size ~30 nm. Similarly, after the pH was adjusted back to 7.0 by acid titration, aggregates of CNIOs formed at pH 4.0 were dissociated to single dispersed constituent particles (see Figure S1 in the Supporting Information). Though the aggregates formed faster and larger after the first cycle of pH modulation, this aggregation−dissociation process was reversible up to 5 cycles. TEM images indicated that no obvious aggregates of CNIOs existed at pH 7.0 after 5 cycles (see Figure S2 in the Supporting Information). UV−vis absorption spectra of CNIO suspensions at different pH conditions revealed higher absorption at pH 4.0 than that at pH 7.0 (see Figure S3 in the Supporting Information), which also confirmed the aggregation of CNIOs at pH 4.0. Both single dispersed CNIOs and aggregated CNIOs showed the characteristic absorption peak at 280 nm, which is attributed to the tryptophan, tyrosine, and cysteine residues in casein.

Because the influence of aggregation on the relaxation rate of single dispersed magnetic nanoparticles provides the potential to optimize the parameter for improved sensitivity and quantification, it has attracted much attention recently.[32,49−55] Early studies showed the relationship between transverse relaxivity, $r_2$, and the size of aggregates, $D$, could be divided into three regimes: (1) motional averaging regime (MAR), where $r_2$ is proportional to $D^2$; (2) static dephasing regime (SDR), where $r_2$ reaches to a maximum plateau, and is independent of $D$; and (3) echo limited regime (ELR), where $r_2$ is proportional to $1/D^2$.[50,56] The initial increase of $r_2$ can be attributed to the interactions between the small magnetic cores inside the aggregates, which enhance the magnetic moment of the nanocrystals, thus increasing the induced magnetic field inhomogenity.[45,57] However, a further increase in the cluster size of aggregates causes exclusion of the water molecules from the inner surface of the particle within polymer coating, altering the relaxation regime.[48,50,56] In most reported cases, significantly increased $r_2$ relaxivity in aggregates or clusters of IO nanoparicles were based on nanoparticles either coated with polymers or encapsulated in micelles or liposomes, where the hydrophobic inner layer of the coating polymers or liposomes may strongly exclude the water molecules from the particle surface.[45,50−54,58] For the CNIOs reported in this study, the MRI contrast enhancing effect was fairly constant and stable over the pH range of 4.0−8.0 (Figure 5b). This unique MRI


dx.doi.org/10.1021/am400713j | ACS Appl. Mater. Interfaces 2013, 5, 4632−4639

property of CNIOs is likely due to the high affinity for water as well as the highly porous and water-permeable structure of the protein coating, which allows for the nearby water molecules to maintain their molecular motion in the similar microenvironment even after they form the loose aggregates at pI 4.0. The loose structure of the CNIO aggregates differs from those compact polymer coated or liposome or micelle-encapsulated multicore nanoparticle clusters previously reported in the literatures. Moreover, the distance between the nanoparticles in the CNIO aggregates is likely long, so that the interaction between each magnetic particle core is weak. Thus we did not observe a change of overall $r_2$ relaxivity of CNIO aggregates comparing to that of CNIO single cores. In fact, the observed constant transverse relaxivity and MRI contrast enhancing effect over the pH range of 4.0−8.0 provided indirect evidence that the high hydrophilicity and low diffusion restraints for water molecules moving in the protein layer contribute to the much higher $r_2$ values of CNIOs. This unique phenomenon in CNIOs may lead to a new approach for developing high transverse relaxivity MRI contrast agents through promoting surface hydrophilicity, not just increasing the nanocrystal size. Nonetheless, further investigation is needed for a better understanding of such properties that contribute to relaxivities and MRI contrast enhancement as new classes of magnetic nanoparticles and surface coating materials are developed for MRI applications.

**Cytotoxicity of CNIOs.** To investigate the biocompatibility, cytotoxicity of CNIOs was evaluated using MTT assay by incubating macrophage RAW264.7 cells with medium containing CNIOs at different concentrations (5−200 $\mu$g Fe/mL) for 24 h. The cell viability was tested by MTT assay and normalized to the control samples. The cells incubated with CNIOs survived even at the highest iron concentration at 200 $\mu$g Fe/mL, showing viability ~90% compared to the control (Figure 6). These results suggested that these newly developed CNIOs are biocompatible and suitable for biomedical applications.

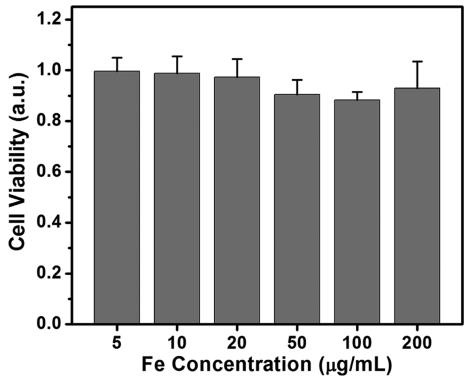


**Figure 6.** Cell viability of RAW264.7 macrophage cells treated with various concentrations of CNIOs for 24 h measured by MTT assay.

**MRI Contrast Enhancement of CNIOs in Mice.** To further test the MRI contrast enhancing capability in vivo, CNIOs were intravenously (i.v.) administered into Balb/c mice at the dosage of 2.5 mg Fe/kg of mouse body weight. $T_2$-weighted MRI was performed before and after injection. As shown in Figure 7a, hypointensities induced by CNIOs can be readily observed in liver and spleen at 20 min after injection. The signal-to-noise ratio (SNR) increased ~76% and ~52% in liver and spleen, respectively. The contrast in liver began to decrease after 24 h of injection (Figure 7b) because of the liver clearance. The contrast enhancement indicated the accumulation of CNIOs in these organs, demonstrating that CNIOs can be potentially used as effective $T_2$-weighted MRI contrast agents. Biodistribution studies revealed the increase of iron concentration in liver and spleen after i.v. injection (see Figure S5 in the Supporting Information). Additionally, Prussian blue staining identified the presence of CNIOs in these organs. However, lower uptake of CNIOs by liver and spleen was observed in comparison with the polymer coated particles (SHP15) with the same size and surface charge (see Figure S6 in the Supporting Information).

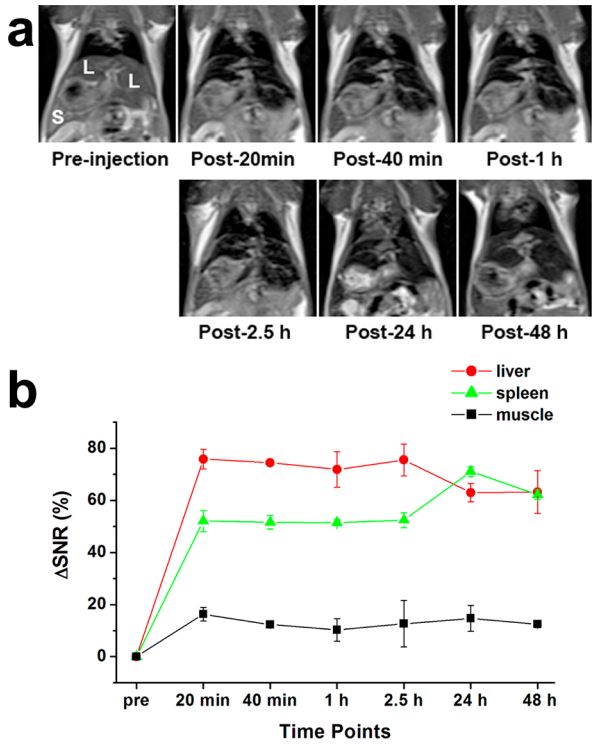


**Figure 7.** (a) $T_2$-weighted MR images of a mouse before and after injection of CNIOs at a dosage of 2.5 mg Fe/kg per mouse body weight; (b) relative MR signal-to-noise ratio (SNR) in liver, spleen and muscle.

**Specific Targeting to Cancer Cells with EGFR Targeted CNIOs.** Specific targeting of ScFvEGFR-CNIOs (with hydrodynamic size ~35.0 nm, see Figure S6 in the Supporting Information) to cancer cells was determined by coincubating cells with ScFvEGFR-CNIOs, followed by Prussian blue staining for iron. Human breast cancer MDA-MB-231 and MCF7 cells were selected as target and nontarget control cell lines. As shown in Figure 8, the cellular uptake of ScFvEGFR-CNIOs by MDA-MB-231 cells (overexpressing EGFR) was significant and in a dose-dependent manner. In comparison, little cellular uptake was observed in MCF7 cells (low level of expressing EGFR) treated with ScFvEGFR-CNIOs.

## CONCLUSIONS

We have produced a new class of protein coated iron oxide nanoparticles using milk protein casein. Through ligand exchange and subsequent encapsulation of magnetic IO nanoparticles with casein, the prepared CNIOs showed


dx.doi.org/10.1021/am400713j | ACS Appl. Mater. Interfaces 2013, 5, 4632−4639

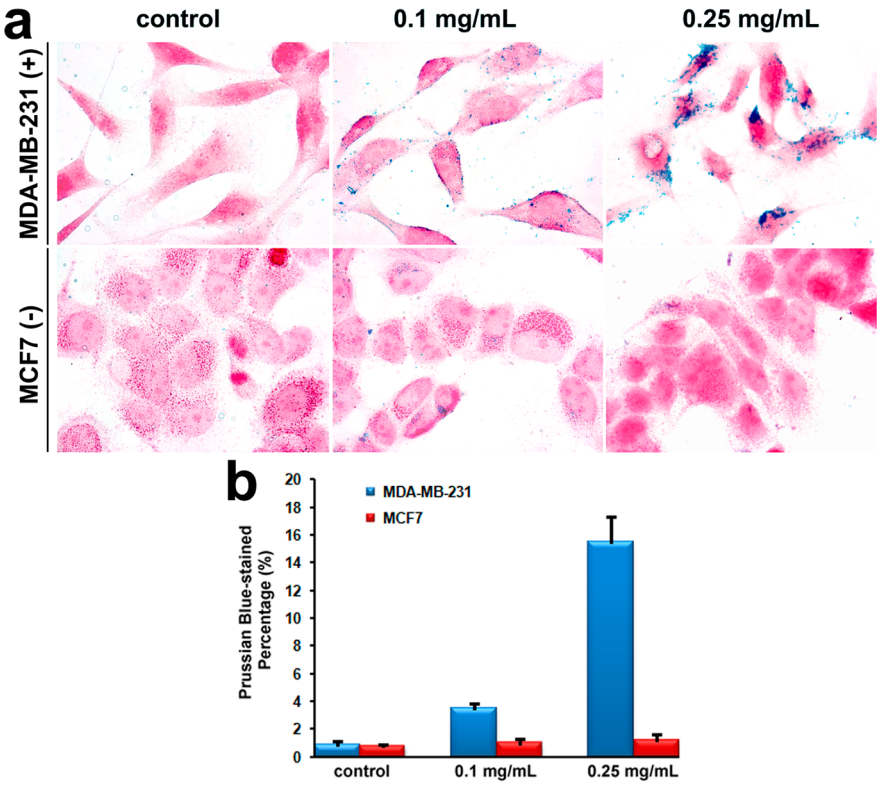


**Figure 8.** (a) Representative microscope images for Prussian blue staining of MDA-MB-231 (overexpressing EGFR) and MCF7 (low level of expressing EGFR) cells after incubated with ScFvEGFR-CNIOs at 37 °C for 4 h, stained IO nanoparticles present as blue dots; (b) Percentages of Prussian blue positive cells analyzed by ImageJ revealed pronounced cellular uptake of ScFvEGFR-CNIOs by MDA-MB-231 cells.

excellent water solubility and stability in the pH range of 5.0–8.0 with a pI of 4.0. Compared with the IO nanoparticles with same hydrophobic IO core but coated with conventional synthetic polymer, these CNIOs exhibited substantially higher relaxivity and improved MRI contrast. Therefore, CNIOs potentially may provide high MRI sensitivity at a reduced dosage. The prepared CNIOs also show pH-responsive properties. Loose and soluble aggregates of CNIOs were formed near the pI ~4.0. However, this was reversible as the aggregates dissociated to monodispersed single core form when the solution pH was adjusted back to 7.0. It is noticed that no significant change was found for the transverse relaxation properties and MRI contrast enhancing effect at a pH range of 4.0 and 7.0. Furthermore, the carboxylic functional groups on the protein coating allow for the conjugation of bioactive moieties, such as biomarker specific targeting ligands. These results have demonstrated that CNIOs may provide a promising new class of MRI contrast agents, and could be extended to other protein-coated nanoconstructs in biomedical applications.

## ■ ASSOCIATED CONTENT

### Supporting Information

(1) Reversible size change, TEM images, and UV–vis absorption at different pH conditions. (2) Magnetic susceptibility measurement and comparisons of CNIO and SPH15. This materials is available free of charge via the Internet at http://pubs.acs.org.

## ■ AUTHOR INFORMATION

### Corresponding Author

*E-mail: hmao@emory.edu.

### Notes

The authors declare no competing financial interest.

## ■ ACKNOWLEDGMENTS

We thank Prof. Xiqun Jiang of Nanjing University for stimulating discussions on the potential use of milk proteins for biomedical applications, and Dr. Gregory Adams of Fox Chase Cancer for providing ScFvEGFR expressing plasmid, and Ms. Heather Price Boldt and Ms. Jessica Paulishen for their assistance in editing and proofreading the manuscript. This work is supported in part by National Institutes of Health (NIH) and National Cancer Institute (NCI)'s in vivo Cellular and Molecular Imaging Center grant (ICMIC; P50CA128301-01A10003 to H.M. and L.Y.), NCI's Cancer Nanotechnology Partnership Project (CNPP) grant (U01CA151810-02 to L.Y. and H.M.), and NCI's R01CA154846-02 (to H.M. and L.Y.).

## ■ ABBREVIATIONS

CN, casein
IO, iron oxide
MRI, magnetic resonance imaging
PAA, poly(acrylic acid)
PEI, polyethylenimine
GSH, glutathione
DMSO, dimethyl sulfoxide
CNIOs, casein-coated iron oxide nanoparticles
DMF, *N*-dimethylformamide
MTT, 3-[4,5-dimethylthiazol-2-yl]-2,5-diphenyltetrazolium bromide
EDC, 1-ethyl-3-[3-dimethylaminopropyl]carbodiimide hydrochloride
Sulfo-NHS, *N*-hydroxysulfosuccinimide

TEM, transmission electron microscope
PTA, phosphotungstic acid
DLS, dynamic light scattering
FTIR, Fourier transform infrared spectroscopy
SI, signal intensity
SNR, signal-to-noise ratio
ScFvEGFR, human EGFR specific single-chain fragment of anti-EGFR antibody
SIO, oligosaccharide-coated iron oxide nanoparticle

## REFERENCES


(1) Mahmoudi, M.; Hosseinkhani, H.; Hosseinkhani, M.; Boutry, S.; Simchi, A.; Journeay, W. S.; Subramani, K.; Laurent, S. *Chem. Rev.* **2011**, *111*, 253.
(2) Schroeder, A.; Heller, D. A.; Winslow, M. M.; Dahlman, J. E.; Pratt, G. W.; Langer, R.; Jacks, T.; Anderson, D. G. *Nat. Rev. Cancer* **2012**, *12*, 39.
(3) Laurent, S.; Bridot, J.-L.; Elst, L. V.; Muller, R. N. *Future Med. Chem.* **2010**, *2*, 427.
(4) Reddy, L. H.; Arias, J. L.; Nicolas, J.; Couvreur, P. *Chem. Rev.* **2012**, *112*, 5818.
(5) Huang, J.; Zhong, X.; Wang, L.; Yang, L.; Mao, H. *Theranostics* **2012**, *2*, 86.
(6) Chen, K.; Xie, J.; Xu, H.; Behera, D.; Michalski, M. H.; Biswal, S.; Wang, A.; Chen, X. *Biomaterials* **2009**, *30*, 6912.
(7) Park, J.-H.; von Maltzahn, G.; Ruoslahti, E.; Bhatia, S. N.; Sailor, M. J. *Angew. Chem., Int. Ed.* **2008**, *47*, 7284.
(8) Tassa, C.; Shaw, S. Y.; Weissleder, R. *Acc. Chem. Res.* **2011**, *44*, 842.
(9) Xu, Y.; Qin, Y.; Palchoudhury, S.; Bao, Y. *Langmuir* **2011**, *27*, 8990.
(10) Zhang, T.; Ge, J.; Hu, Y.; Yin, Y. *Nano Lett.* **2007**, *7*, 3203.
(11) Duan, H.; Kuang, M.; Wang, X.; Wang, Y. A.; Mao, H.; Nie, S. *J. Phys. Chem. C* **2008**, *112*, 8127.
(12) Zhang, B.; Li, Q.; Yin, P.; Rui, Y.; Qiu, Y.; Wang, Y.; Shi, D. *ACS Appl. Mater. Interfaces* **2012**, *4*, 6479.
(13) Meldrum, F. C.; Wade, V. J.; Nimmo, D. L.; Heywood, B. R.; Mann, S. *Nature* **1991**, *349*, 684.
(14) Valero, E.; Tambalo, S.; Marzola, P.; Ortega-Munoz, M.; Lopez-Jaramillo, F. J.; Santoyo-Gonzalez, F.; de Dios Lopez, J.; Delgado, J. J.; Calvino, J. J.; Cuesta, R.; Dominguez-Vera, J. M.; Galvez, N. *J. Am. Chem. Soc.* **2011**, *133*, 4889.
(15) Meldrum, F. C.; Heywood, B. R.; Mann, S. *Science* **1992**, *257*, 522.
(16) Fan, K.; Cao, C.; Pan, Y.; Lu, D.; Yang, D.; Feng, J.; Song, L.; Liang, M.; Yan, X. *Nat. Nanotechnol.* **2012**, *7*, 459.
(17) Lee, J.-h.; Jung, M. J.; Hwang, Y. H.; Lee, Y. J.; Lee, S.; Lee, D. Y.; Shin, H. *Biomaterials* **2012**, *33*, 4861.
(18) Sangeetha, J.; Philip, J. *Colloids Surf., A* **2012**, *406*, 52.
(19) Farrell, H. M.; Jimenez-Flores, R.; Bleck, G. T.; Brown, E. M.; Butler, J. E.; Creamer, L. K.; Hicks, C. L.; Hollar, C. M.; Ng-Kwai-Hang, K. F.; Swaisgood, H. E. *J. Dairy Sci.* **2004**, *87*, 1641.
(20) Modler, H. W. *J. Dairy Sci.* **1985**, *68*, 2195.
(21) Livney, Y. D. *Curr. Opin. Colloid Interface Sci.* **2010**, *15*, 73.
(22) Holt, C.; Horne, D. S. *Neth. Milk Dairy J.* **1996**, *50*, 85.
(23) Horne, D. S. *Curr. Opin. Colloid Interface Sci.* **2006**, *11*, 148.
(24) Holt, C.; de Kruif, C. G.; Tuinier, R.; Timmins, P. A. *Colloids Surf., A* **2003**, *213*, 275.
(25) Farrell, H. M., Jr.; Malin, E. L.; Brown, E. M.; Qi, P. X. *Curr. Opin. Colloid Interface Sci.* **2006**, *11*, 135.
(26) Dalgleish, D. G. *Soft Matter* **2011**, *7*, 2265.
(27) Flett, K. L.; Corredig, M.; Goff, H. D. *J. Food Sci.* **2010**, *75*, 433.
(28) Holt, C. *Adv. Protein Chem.* **1992**, *43*, 63.
(29) Dalgleish, D. G. *J. Dairy Sci.* **1998**, *81*, 3013.
(30) Song, F.; Zhang, L.-M.; Yang, C.; Yan, L. *Int. J. Pharm.* **2009**, *373*, 41.
(31) Sahu, A.; Kasoju, N.; Bora, U. *Biomacromolecules* **2008**, *9*, 2905.
(32) Liu, C.; Yao, W.; Zhang, L.; Qian, H.; Wu, W.; Jiang, X. *Chem. Commun.* **2010**, *46*, 7566.
(33) Zimet, P.; Rosenberg, D.; Livney, Y. D. *Food Hydrocolloids* **2011**, *25*, 1270.
(34) Bachar, M.; Mandelbaum, A.; Portnaya, I.; Perlstein, H.; Even-Chen, S.; Barenholz, Y.; Danino, D. *J. Controlled Release* **2012**, *160*, 164.
(35) Elzoghby, A. O.; Samy, W. M.; Elgindy, N. A. *J. Controlled Release* **2012**, *161*, 38.
(36) Abd El-Salam, M. H.; El-Shibiny, S. *Int. J. Dairy Technol.* **2012**, *65*, 13.
(37) Huang, J.; Xie, J.; Chen, K.; Bu, L.; Lee, S.; Cheng, Z.; Li, X.; Chen, X. *Chem. Commun.* **2010**, *46*, 6684.
(38) Sugisawa, H.; Edo, H. *J. Food Sci.* **1966**, *31*, 561.
(39) Sun, X. M.; Li, Y. D. *Angew. Chem., Int. Ed.* **2004**, *43*, 597.
(40) Yu, W. W.; Falkner, J. C.; Yavuz, C. T.; Colvin, V. L. *Chem. Commun.* **2004**, 2306.
(41) Zhou, Y.; Daryl, C.; Zou, H.; Hayes, M. E.; Adams, G. P.; Kirpotin, D. B.; JD, M. *J. Mol. Biol.* **2007**, *371*, 934.
(42) Yang, L.; Mao, H.; Wang, Y. A.; Cao, Z.; Peng, X.; Wang, X.; Duan, H.; Ni, C.; Yuan, Q.; Adams, G.; Smith, M. Q.; Wood, W. C.; Gao, X.; Nie, S. *Small* **2009**, *5*, 235.
(43) Peng, X.; Wang, Y.; Huang, D.; Wang, Y.; Shin, H. J.; Chen, Z.; Spewak, M. B.; Mao, H.; Wang, X.; Wang, Y.; Chen, Z.; Nie, S.; Shin, D. M. *Acs Nano* **2011**, *5*, 9480.
(44) Paquet, C.; de Haan, H. W.; Leek, D. M.; Lin, H.-Y.; Xiang, B.; Tian, G.; Kell, A.; Simard, B. *ACS Nano* **2011**, *5*, 3104.
(45) Poeselt, E.; Kloust, H.; Tromsdorf, U.; Janschel, M.; Hahn, C.; Masslo, C.; Weller, H. *ACS Nano* **2012**, *6*, 1619.
(46) Lartigue, L.; Innocenti, C.; Kalaivani, T.; Awwad, A.; Duque, M. d. M. S.; Guari, Y.; Larionova, J.; Guerin, C.; Montero, J.-L. G.; Barragan-Montero, V.; Arosio, P.; Lascialfari, A.; Gatteschi, D.; Sangregorio, C. *J. Am. Chem. Soc.* **2011**, *133*, 10459.
(47) Jain, T. K.; Richey, J.; Strand, M.; Leslie-Pelecky, D. L.; Flask, C. A.; Labhasetwar, V. *Biomaterials* **2008**, *29*, 4012.
(48) Gossuin, Y.; Gillis, P.; Hocq, A.; Vuong, Q. L.; Roch, A. *Wiley Interdiscip. Rev. Nanomed. Nanobiotechnol.* **2009**, *1*, 299.
(49) Roch, A.; Gossuin, Y.; Muller, R. N.; Gillis, P. *J. Magn. Magn. Mater.* **2005**, *293*, 532.
(50) Balasubramaniam, S.; Pothayee, N.; Lin, Y.; House, M.; Woodward, R. C.; St Pierre, T. G.; Davis, R. M.; Riffle, J. S. *Chem. Mater.* **2011**, *23*, 3348.
(51) Perez, J. M.; Josephson, L.; O'Loughlin, T.; Hogemann, D.; Weissleder, R. *Nat. Biotechnol.* **2002**, *20*, 816.
(52) Larsen, B. A.; Haag, M. A.; Serkova, N. J.; Shroyer, K. R.; Stoldt, C. R. *Nanotechnology* 2008, *19*.
(53) Osborne, E. A.; Jarrett, B. R.; Tu, C.; Louie, A. Y. *J. Am. Chem. Soc.* **2010**, *132*, 5934.
(54) Kaittanis, C.; Santra, S.; Santiesteban, O. J.; Henderson, T. J.; Perez, J. M. *J. Am. Chem. Soc.* **2011**, *133*, 3668.
(55) Chen, H.; Yeh, J.; Wang, L.; Khurshid, H.; Peng, N.; Wang, A. Y.; Mao, H. *Nano Res.* **2010**, *3*, 852.
(56) Tromsdorf, U. I.; Bigall, N. C.; Kaul, M. G.; Bruns, O. T.; Nikolic, M. S.; Mollwitz, B.; Sperling, R. A.; Reimer, R.; Hohenberg, H.; Parak, W. J.; Forster, S.; Beisiegel, U.; Adam, G.; Weller, H. *Nano Lett.* **2007**, *7*, 2422.
(57) Qiu, P.; Jensen, C.; Charity, N.; Towner, R.; Mao, C. *J. Am. Chem. Soc.* **2010**, *132*, 17724.
(58) Cha, J.; Kwon, Y.-S.; Yoon, T.-J.; Lee, J.-K. *Chem. Commun.* **2013**, *49*, 457.